A novel decision making approach for benchmarking the service quality of smart community health centers

Li, Hao ; Li, Jinlin ; Dietl, Helmut

Abstract: The purpose of this research is to develop a novel approach to benchmark smart community health centers in order to achieve continuous improvement of service quality. Three methods are presented: the fuzzy DEMATEL method is used to determine the criteria weights, the fuzzy ELECTRE III method is employed to obtain the ranking of smart community health centers, and IPA (Importance-Performance Analysis) is employed to formulate improvement strategies. The proposed approach clearly identifies the strengths and weakness of each smart community health center by ranking its performance with respect to a system of five service quality criteria. In addition, IPA is able to develop the most effective improvement strategies for each smart community health center. The proposed approach was applied to five smart community health centers in Beijing and service strengths and weakness are discussed. The proposed approach has three notable advantages. First, the novel approach can address ambiguity and uncertainty in the process of decision making. Second, interdependent relationships among the evaluation criteria are analyzed by the fuzzy DEMATEL method, so that the weights obtained are more in line with reality. Third, the fuzzy ELECTRE III method considers non-compensatory behavior for service quality comparisons among smart community health centers. The novel fuzzy-based approach presented in this paper is a powerful and highly effective tool to benchmark smart community health centers and develop successful improvement strategies of service quality.

DOI: https://doi.org/10.1109/ACCESS.2020.3037769

Monitored Reconstruction: Computed Tomography as an Anytime Algorithm

Article *in* IEEE Access · June 2020

DOI: 10.1109/ACCESS.2020.3002019

5 authors, including:

Konstantin Bulatov
Federal Research Center "Computer Science and Control" of the Russian Academ…
28 PUBLICATIONS **115** CITATIONS
SEE PROFILE

Marina Chukalina
Russian Academy of Sciences
96 PUBLICATIONS **844** CITATIONS
SEE PROFILE

Alexey V. Buzmakov
Russian Academy of Sciences
88 PUBLICATIONS **298** CITATIONS
SEE PROFILE

Dmitry Nikolaev
The Institute for Information Transmission Problems
143 PUBLICATIONS **631** CITATIONS
SEE PROFILE

IEEE Access
Multidisciplinary | Rapid Review | Open Access Journal

Date of publication xxxx 00, 0000, date of current version xxxx 00, 0000.

Digital Object Identifier 00000/00000.00000

Monitored Reconstruction: Computed Tomography as an Anytime Algorithm

KONSTANTIN BULATOV[1, 4], (Member, IEEE), MARINA CHUKALINA[2, 3, 4], (Member, IEEE), ALEXEY BUZMAKOV[2, 4], (Member, IEEE), DMITRY NIKOLAEV[3, 4], (Member, IEEE), and VLADIMIR V. ARLAZAROV[1, 4], (Member, IEEE)

[1]Federal Research Center "Computer Science and Control" of Russian Academy of Sciences, Moscow, Russia
[2]Federal Scientific Research Center "Crystallography and Photonics" of Russian Academy of Sciences, Moscow, Russia
[3]Institute for Information Transmission Problems of Russian Academy of Sciences (Kharkevich Institute), Moscow, Russia
[4]Smart Engines Service LLC, Moscow, Russia

Corresponding author: Konstantin Bulatov (e-mail: kbulatov@smartengines.com).

This work was partially financially supported by Russian Foundation for Basic Research, projects 18-29-26020 and 20-07-00934.

ABSTRACT Computed tomography is an important technique for non-destructive analysis of an object's internal structure, relevant for scientific studies, medical applications, and industry. Pressing challenges emerging in the field of tomographic imaging include speeding up reconstruction, reducing the time required to obtain the X-ray projections, and reducing the radiation dose imparted to the object. In this paper, we introduce a model of a monitored reconstruction process, in which the acquiring of projections is interspersed with image reconstruction. This model allows to examine the tomographic reconstruction process as an anytime algorithm and consider a problem of finding the optimal stopping point, corresponding to the required number of X-ray projections for the currently scanned object.

We outline the theoretical framework for the monitored reconstruction, propose ways of constructing stopping rules for various reconstruction quality metrics and provide their experimental evaluation. Due to stopping at different times for different objects, the proposed approach allows to achieve a higher mean reconstruction quality for a given mean number of X-ray projections. Conversely, fewer projections on average are used to achieve the same mean reconstruction quality.

INDEX TERMS Anytime algorithms, computed tomography, dose reduction, monitored reconstruction, optimal stopping, x-ray tomography.

I. INTRODUCTION

A. COMPUTED TOMOGRAPHY AND ITS APPLICATIONS

Computed tomography (CT) is a powerful non-destructive technique for constructing detailed images of internal object areas [1]. The target object is probed with X-rays at different angles. The tomographic projections are collected relying on the property of X-rays attenuation as they traverse the matter. Attenuation is the reduction of the intensity of an X-ray beam, which is used to create an image. The attenuation may be caused by absorption or by deflection (scattering) of photons from the beam and can be affected by beam energy and the atomic number of the absorber [2].

Computed tomography has important applications in such fields as industry, physics, chemistry [3], biology [4], medicine, and others. Analysis of a three-dimensional internal structure of objects is required for the study of multi-material components [5], for characterization of object's properties [6], or to analyze nanostructures [7], [8]. More problem-specific applications include archaeology, where computed tomography is used for the analysis of precious artifacts [9], or to read historical manuscripts which could not be manually handled [10]. Increased international trade requires automatization of cargo inspection, which could be performed using tomographic analysis [11], and there are studies of CT application for airport luggage inspection systems [12]. Medical CT scanning is widely used to diagnose muscle and bone disorders, to pinpoint the location of tumours, and to monitor the effectiveness of certain treatments. Active studies continue to improve both the technical side and the diagnostic side of the medical CT applications [13].

Along with the development of techniques and protocols for the study of stationary objects, another actively developed direction is the study of dynamic objects, or the so-called 4D-tomography [14]. 4D reconstruction techniques in a medical field allows studying the organs which are in continuous motion, such as lungs [15], [16] and heart [17]–[19].

This article has been accepted for publication in a future issue of this journal, but has not been fully edited. Content may change prior to final publication. Citation information: DOI 10.1109/ACCESS.2020.3002019, IEEE Access

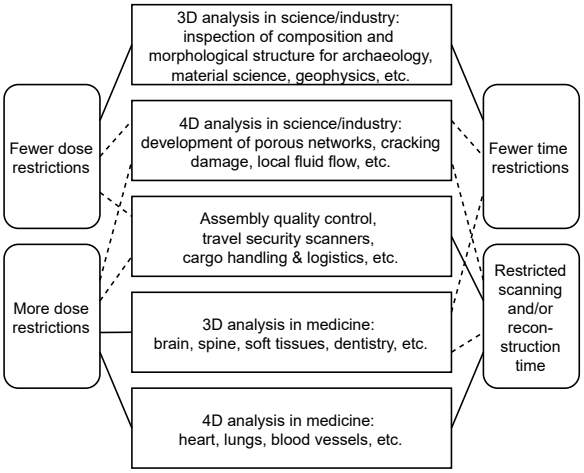

FIGURE 1. Computed tomography applications in reference to the restrictions on time and radiation dose.

Industrial applications of 4D tomography include monitoring of the development of porous networks [20], cracking damage [21], local fluid flow [22], and more [23].

An important issue of the CT applications is the time required to obtain X-ray projections and to perform the image reconstruction. It is particularly relevant in the medical field, both for diagnostic purposes and for more advanced applications such as guiding surgical operations [24]. Reconstruction speed requirement is also present in the industry, for such applications as quality control on assembly lines [25]. Another important issue of computed tomography is radiation exposure, since only a small class of studied objects has radiation resistance. The decrease of imparted dose during tomographic scanning is of great importance, particularly in the medical field [26], [27]. Different applications of computed tomography grouped by the time and radiation exposure requirements are presented in Figure 1.

B. MINIMIZING THE DOSE

The amount of X-ray radiation which is absorbed during the imaging process contributes to the object's radiation dose. In spite of there being an understood need to reduce the absorbed radiation dose, within an ALARA concept (As Low as Reasonably Achievable) discussed on a multidisciplinary conference in 2001 [28], there is no consensus regarding how the dose should be expressed and measured. Multiple approaches are used to describe the CT-delivered dose, the most relevant being absorbed dose, effective dose, background equivalent radiation time [29], and CT dose index (CTDI) [30]. The absorbed dose is the energy absorbed per unit of mass and it is measured in grays (Gy). The unit of measurement for the whole-body radiation dose (called the "effective dose") is the millisievert (mSv). Medical doctors use the "effective dose" when they talk about the risk of radiation exposure of the entire body, as it takes into account how sensitive different tissues are to the radiation. The effective dose allows a rough comparison of different CT scenarios and scanning techniques, but it provides only an approximate estimate of the true risk. For more precise risk estimation, the organ dose is the preferred figure. Organ doses can be calculated or measured using anthropomorphic phantoms [31]. In [32] authors consider ALARA on a local level to be met using the lowest possible exposure with the available equipment and software while maintaining diagnostic interpretability.

The radiation dose depends on a large number of factors [30]. The most important are the number of projection angles, the X-ray tube current and voltage, the size of the object, the axial scan range, the scan pitch (the degree of overlap between adjacent CT slices), scanning time and the specific design of the tomograph. Requirements to the new generation of tomography scanners are defined by advanced measurement protocols that prevent reproductive and apoptotic death of cells after radiation injury.

Along with the optimization of set-ups based on the use of a gantry [2], scanners are created with a controlled collection of projections with an arbitrary angle. This is implemented in two main ways: either X-ray beams are registered by multiple source-detector pairs for data acquisition [33] or the X-ray source-point is swept electronically [34]. It is always the case that the relative noise in CT images will increase as the radiation dose decreases, which means that there will always be a trade-off between the need for low-noise images and the desire to achieve low doses of radiation [35]. If the tube current and voltage are fixed, it is possible to decrease the radiation dose by decreasing the exposure time or decreasing the number of projection angles.

Overall, new optimized protocols and procedures are put in place, based both on the new generation of tomographic scanners and on adaptive iterative reconstruction software, in an effort to reduce the mean imparted dose. However, the quality of the reconstructed images given the same protocol could be different for different objects. And if all objects (e.g. all medical patients) are scanned using the same protocol, then some will absorb an optimal radiation dose (that is, in relation to the required reconstruction quality), some – in excess, and some will get a dose which is insufficient to produce an acceptable reconstruction and will have to be subjected to a re-scan with a modified setting.

C. RECONSTRUCTION AS AN ANYTIME ALGORITHM

In this paper, we propose to look at the CT scanning procedure as an anytime algorithm. Anytime algorithms as a way of thinking about algorithms with quantifiable goals are useful when the cost of computation (whether in terms of time or other quantities) is comparable, or at least relevant, in relation to the cost of error. Intelligent systems such as decision support systems [36] and computer vision systems [37]–[39] use the model of anytime algorithms to represent and manage the trade-off between the quality of the result and the time required to obtain it. If the tomographic procedure is not broken down into separate stages scanning and reconstruction, the tomographic scanning cost can be

either expressed in terms of time required to collect the projections, or in terms of radiation dose delivered to the object. If the reconstruction process is monitored during the process of obtaining projections, the decision to stop the scanning process may be made when the sufficient reconstructed image quality is achieved. We call this approach a monitored reconstruction.

The goal of this paper is to build a model of the monitored reconstruction process and evaluate its feasibility, advantages, and disadvantages.

The rest of the paper is organized as follows. Section II contains a theoretical framework for the monitored reconstruction process, formulation of the main hypotheses and optimization tasks, and construction of the stopping rules. Section III presents an experimental evaluation of the process and shows the advantages of monitored reconstruction with different stopping time for different objects. Section IV presents the discussion of the obtained results.

II. FRAMEWORK

The desired properties of anytime algorithms are formulated and categorized in [40], and one of the most important ones is monotonicity, which requires the quality of the result to be a non-decreasing function of time (computational cost) and input quality. Putting aside the input quality, if we consider partial reconstruction in the tomographic imaging process, each based on a limited number of currently acquired projections, it is natural to expect the reconstruction results to "improve" over time. Thus, we can consider such imaging process as an anytime algorithm. Let us define such process as a *monitored reconstruction* process. In this section, we describe a model of such a process and analyze its properties.

A. PROJECTIONS AND PARTIAL RECONSTRUCTION

Let us assume that the physical properties of the tomography setup are fixed, including the protocol for acquiring projections, dimensions, resolution, etc. Given a fixed experimental setup consider a sequential tomographic imaging process of an object $\theta \in \Theta$ (the imaging target). During the process, we observe a sequence of projections $\mathbf{X} = (X_1, X_2, ...)$ according to a fixed experimental protocol. Each X_i can be viewed as a random vector dependent on θ, which has a sample space χ and encodes both the projection and the angle with which this projection is acquired.

Given a sequence of projections $(x_1, x_2, \dots, x_n) \in \chi^n$ a tomographic reconstruction can be performed, thus obtaining a reconstruction result $R_n(x_1, x_2, \dots, x_n)$. For the purposes of the constructed anytime algorithm model we will assume that the reconstruction $R_n(x_1, \dots, x_n)$ is performed after each projection $X_n = x_n$ is acquired. The final goal is to obtain a reconstruction result with the lowest value of the reconstruction error $\epsilon(R_n(x_1, \dots, x_n), \theta)$, which is defined for any object $\theta \in \Theta$ and all possible reconstruction results. In terms of anytime algorithms by defining an error function ϵ it is stated that the algorithm has the property of measurable quality [40]. However this does not necessarily mean that it has recognizable quality – the precise value of the current reconstruction error $\epsilon(R_n(x_1, \dots, x_n), \theta)$ might not be possible to determine at run time. The assumed property of monotonicity implies that the value of $\epsilon(R_n(x_1, \dots, x_n), \theta)$ decreases over time (that is, as n increases).

Considering the differences in the quality of partial reconstructions implies that the acquired projections also have a cost. The need to balance the error of the currently available reconstruction result and the cost of obtaining it brings forward the problem of optimal stopping – determining the moment when the acquisition of projections should stop and the current reconstruction result should be considered final.

It is important that if given a fixed error function ϵ and a fixed experimental setup the speed of the error value $\epsilon(R_n(x_1, \dots, x_n), \theta)$ has the same decrease speed for all $\theta \in \Theta$, the stopping rules are not required at all – the number of projections required to reach a certain level of error would be the same. Thus, to even consider stopping rules which would allow stopping at different process stages, depending on the collected projections and tomographical reconstruction results, we need to put forward the following hypothesis:

Hypothesis 1 (H1) The decrease speed of the error value $\epsilon(R_n(x_1, \dots, x_n), \theta)$ depends on the object θ.

B. PROJECTION COST AND STOPPING RULES

The notation used in this subsection roughly follows the works [41], [42] which contain a comprehensive description of optimal stopping problems formalization.

To reflect the cost of acquired projections, whether in terms of time or dosage, and the cost of computation required to perform partial reconstructions, a sequence of real-valued cost functions is defined: $\mathbf{c} = (c_0, c_1(x_1), c_2(x_1, x_2), \dots)$. Each cost function c_n has a domain χ^n and denotes the total cost of acquiring projections $X_1 = x_1, \dots, X_n = x_n$ and obtaining a reconstruction result $R_n(x_1, \dots, x_n)$, relative to the cost of the reconstruction error. We will assume that the cost of taking no observations at all is zero (i.e. $c_0 = 0$), taking additional observations always costs a non-negative amount, i.e. $c_n(x_1, \dots, x_n) < c_{n+1}(x_1, \dots, x_n, x_{n+1})$, and the cost does not converge to any finite limit, i.e. $c_n(x_1, \dots, x_n) \to \infty$ with $n \to \infty$. The total loss $L_n(x_1, \dots, x_n)$ of acquiring n projections and taking $R_n(x_1, \dots, x_n)$ as the final reconstruction result is a sum of the reconstruction error and the cost of obtained observations:

$$L_n(x_1, \dots, x_n) = \\ = \epsilon(R_n(x_1, \dots, x_n), \theta) + c_n(x_1, \dots, x_n). \quad (1)$$

A stopping rule is defined as a sequence of functions $\boldsymbol{\phi} = (\phi_0, \phi_1(x_1), \phi_2(x_1, x_2), \dots)$ with ϕ_n having a domain χ^n and $0 \leq \phi_n(x_1, \dots, x_n) \leq 1$ for all n. The value of $\phi_n(x_1, \dots, x_n)$ represents the conditional probability of stopping given that n projections has been acquired and $X_1 = x_1, \dots, X_n = x_n$. The value ϕ_0 is constant and represents the probability of acquiring no projections. With a given

This article has been accepted for publication in a future issue of this journal, but has not been fully edited. Content may change prior to final publication. Citation information: DOI 10.1109/ACCESS.2020.3002019, IEEE Access

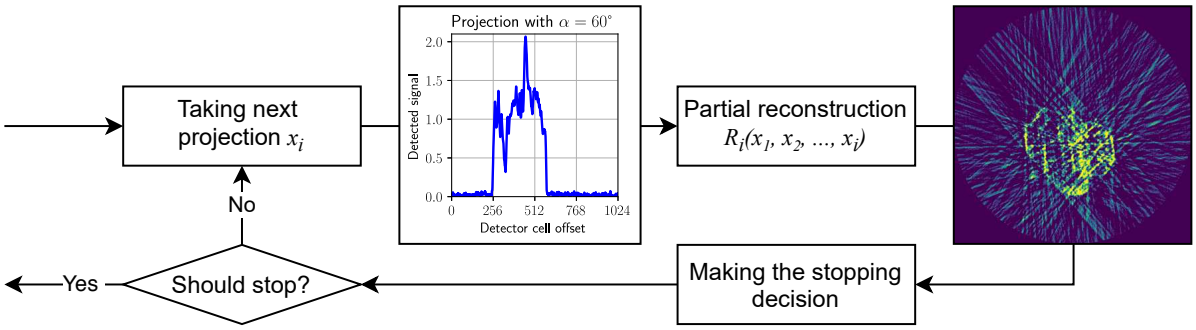

FIGURE 2. Monitored tomographic reconstruction scheme.

stopping rule ϕ a random variable N can be defined, which represents the random stopping time. Stopping rule ϕ and random stopping time N are related as follows:

$$\begin{aligned}&\phi_n(x_1, \dots, x_n) = \\ &\quad = \mathrm{P}\left(N = n \mid N \geq n, X_1 = x_1, \dots, X_n = x_n\right). \end{aligned} \quad (2)$$

The probability mass function of N given the obtained observations $X_1 = x_1, X_2 = x_2, \dots$ is denoted as $\boldsymbol{\psi} = (\psi_0, \psi_1(x_1), \dots, \psi_\infty(x_1, x_2, \dots))$, where

$$\begin{aligned}&\psi_n(x_1, \dots, x_n) = \mathrm{P}(N = n \mid X_1 = x_1, \dots, X_n = x_n), \\ &\psi_\infty(x_1, x_2, \dots) = \mathrm{P}(N = \infty | X_1 = x_1, X_2 = x_2, \dots).\end{aligned} \quad (3)$$

The stopping time probability mass functions $\boldsymbol{\psi}$ are related to the stopping rule $\boldsymbol{\phi}$ as follows:

$$\begin{aligned}&\psi_0 = \phi_0, \\ &\psi_n(x_1, \dots, x_n) = \\ &\qquad = \phi_n(x_1, \dots, x_n) \prod_{i=0}^{n-1} (1 - \phi_i(x_1, \dots, x_i)), \\ &\psi_\infty(x_1, x_2, \dots) = 1 - \sum_{n=0}^{\infty} \psi_n(x_1, \dots, x_n).\end{aligned} \quad (4)$$

The stopping problem involves choosing a stopping rule ϕ which would minimize the expected loss $V(\phi)$, which can be expressed as follows:

$$V(\boldsymbol{\phi}) = \mathrm{E}\left(\sum_{n=0}^{=\infty} \psi_n(X_1, \dots, X_n) L_n(X_1, \dots, X_n)\right), \quad (5)$$

where the "$= \infty$" indicates the summation over values of n from 0 to ∞, including ∞. In terms of the random stopping time N the expected loss can be expressed as follows:

$$V(\boldsymbol{\phi}) = \mathrm{E}(L_N(X_1, \dots, X_N)). \quad (6)$$

The solution to the stopping problem (6) defines the time when the monitored reconstruction process should be stopped, i.e. when the reconstructed image quality is sufficient with respect to the expended cost.

The introduction of stopping rules concludes the full model of the monitored tomographic reconstruction process. The scheme of the constructed model is presented in Figure 2.

For the sake of clarity in the subsequent sections let us treat L_n, R_n, c_n as synonyms of $L_n(x_1, \dots, x_n)$, $R_n(x_1, \dots, x_n)$, and $c_n(x_1, \dots, x_n)$ respectively.

C. FROM ANYTIME TO ANYDOSE

By incorporating the time required to acquire the projections $x_1, \dots, x_n$ and the time required to produce a reconstruction R_n using some fixed reconstruction algorithm into the cost functions c_n we obtain a model of the tomographic imaging process as an anytime algorithm in its general sense. By solving the stopping problem we can reach the required level of the reconstruction error (in terms of the function ϵ) in the shortest time on average, and, conversely, obtain on average the lowest reconstruction error given the same measurement time.

Within the scope of anytime algorithms, the cost functions c_n are mostly associated with measurement time, which in our case includes the time required to collect the projections and to reconstruct the image. If an integral reconstruction technique, such as FBP (Filtered Back Projection) [43], is used, then the reconstruction time and projection collection time could be considered commensurable, and the monitored reconstruction process with FBP may be regarded as an anytime algorithm, capable of delivering improved reconstruction results over time, and with the ability of stopping the process when the result becomes satisfactory.

Integral reconstruction techniques produce poor reconstruction results if only a small amount of projections is available, or if the projections have low contrast and poor signal-to-noise ratio. Algebraic techniques [44] have an advantage in this regard, but they have a significantly higher computational complexity [45]. Algebraic methods are iterative and the computational time for a single iteration is comparable with FBP. Monitored reconstruction process with algebraic methods is possible if the algorithms are modified such that the iterations are resumed from the previous state taking into account the newly acquired projections.

An interesting special case presents itself if we disregard the time required to acquire the projections and to perform reconstruction, and focus instead on the radiation dose alone. In this case, the process can be viewed as an "anydose" algorithm, where the optimal stopping problems deals with

This article has been accepted for publication in a future issue of this journal, but has not been fully edited. Content may change prior to final publication. Citation information: DOI 10.1109/ACCESS.2020.3002019, IEEE Access

joint optimization of the reconstruction quality and radiation dose required to obtain it. In the simplest case if each projection imparts a fixed dose $c > 0$ and the exposure between projections is negligible, the cost functions can be defined as follows:

$$c_n(x_1, \dots, x_n) = n \cdot c. \tag{7}$$

The stopping problem (6) with the observation cost function (7) is to choose a stopping rule which would allow reaching the desired reconstruction quality with the minimal average number of acquired projections, i.e. the minimal imparted dose.

D. ERROR METRICS

Given a fixed experimental setup in order to consider the optimal stopping problem (6) we need to define the reconstruction error function $\epsilon(R_n, \theta)$ for an arbitrary object θ.

The reconstruction error is usually defined either in terms of the similarity between the reconstructed image and the ground truth (i.e. the "ideal" reconstruction result $R^*(\theta)$) or in terms of the reconstructed image quality and suitability for further analysis. A multitude of approaches exists with many task-oriented variations [46]. Some of the methods of describing the reconstructed image quality include the analysis of its spatial resolution, noise level, or characteristic reconstruction artifacts [47]. Some image quality metrics try to mimic the human perception and either predict the perceived image quality or perceived similarity between two images. his category includes such metrics as SSIM [48], ISSIM [49], DVQ [50] and others. Each of these metrics estimate in one way or another the expressiveness of object features in the image.

When we are focusing on the anytime and "anydose" aspects of the imaging process, regardless of how the reconstruction error is defined, it always has two distinct components. The first component is related to the scanning setup, the properties of the object, settings of the emitter and the detector, and the algorithm which is used to reconstruct an image using the collected projections. The second component is related to the number of used projections – the fewer projections are used, the higher the error value would be. The monitored reconstruction process does not change the factors which influence the first component: the scanning protocol is fixed, as well as the reconstruction algorithm. However, different solutions for the stopping problem (6) will lead to a different number of projections used for different objects.

Let us consider a partial reconstruction result R_n which was obtained during the monitored tomographic reconstruction process, and which has low quality, i.e. there are artifacts which render the image useless for further analysis, such as medical diagnostics. Does that mean that the process should continue, and more projections should be acquired for the image to improve? Or does that mean that the process should be stopped, and some other experimental parameters need to be changed? To answer these questions one has to consider not the absolute image quality, but rather how much the image would change if more projections are obtained.

With that in mind, in the scope of this paper, we will analyze how well the partial reconstruction results R_n estimate the "ideal" reconstruction result $R^*(\theta)$, in terms of the absolute and relative estimation errors. We considered three simple error functions, all of them based on an ℓ_2 norm in the space of reconstruction results, interpreted as single-channel images with real-valued pixels:

1) RSRE: root square reconstruction error, or an absolute error in terms of the ℓ_2 norm:
$$\mathrm{RSRE}(R_n, \theta) = \|R_n - R^*(\theta)\|_2; \tag{8}$$
2) NRSRE: a normalized version of RSRE, or a relative error in terms of the ℓ_2 norm:
$$\mathrm{NRSRE}(R_n, \theta) = \frac{\|R_n - R^*(\theta)\|_2}{\|R^*(\theta)\|_2}; \tag{9}$$
3) S-RSRE: a normalization of RSRE in relation to the sum $S(R^*(\theta))$ of pixel values of the "ideal" image:
$$\text{S-RSRE}(R_n, \theta) = \frac{\|R_n - R^*(\theta)\|_2}{S(R^*(\theta))}. \tag{10}$$

While the comparison of reconstructed images using RSRE error (8) is the most straightforward way, employing various normalization might be beneficial for the analysis of the effects of image artifacts and noise. The most natural normalization NRSRE (9) is defined in relation to the ℓ_2 of the target image [51]. The downside of this normalization presents itself when the normalization parameter $\|R^*(\theta)\|_2$ needs to be estimated at a given process stage with a limited number of acquired measurements, as the currently obtained projections cannot be used to calculate the ℓ_2 norm of the target image, and some prediction algorithms need to be involved (see subsection II-E). For this reason we also consider a second type of normalization (10) based on the Radon invariant – the sum of all pixel values of the reconstructed image [52]. This value corresponds to the sum of signal values in each projection, independent from the angle, barring the noise. Thus the value of $S(R^*(\theta))$ can be estimated on any stage of the process using the available projections.

In a traditional tomographical imaging process the number of projections which would be taken before the reconstruction is known in advance. In the monitored reconstruction case, we can also assume that the capturing protocol defines a natural stopping point at the stage $n = T$, where all projections are acquired. Thus the last reconstruction result R_T is the one obtainable with all projections scheduled in the experiment. In order to analyze the specific impact of the stopping rules, our goal is to measure the error component which is related to the number of used projections. To achieve that, we can regard the last reconstruction result R_T instead of the ground truth for the stopping problem. This would mean that if our error function value reaches zero, the obtained reconstruction result is as good as it can get with a given measurement protocol.

This article has been accepted for publication in a future issue of this journal, but has not been fully edited. Content may change prior to final publication. Citation information: DOI 10.1109/ACCESS.2020.3002019, IEEE Access

E. SOLVING THE STOPPING PROBLEM

If we assume that there is a stage $n = T$ where the process must stop regardless of the obtained result, the problem (6) can be described as a finite horizon stopping problem.

For finite horizon stopping problems with known distributions of $X_1, X_2, ...$ and known functions L_n (1), the general approach for finding an optimal stopping rule is backwards induction [42], [53]. A special case of the optimal stopping problems are *monotone stopping problems* [42], [54], for which the backwards induction approach leads to a formulation of a family of optimal stopping rules denoted as *k-stage look-ahead rules* [42].

For brevity let us denote as $\mathrm{E}_n(\cdot)$ the conditional expectation $\mathrm{E}(\cdot|X_1 = x_1, \dots, X_n = x_n)$ of a random variable given that the first n observations are taken. Let A_n denote the event $\{L_n \le \mathrm{E}_n(L_{n+1})\}$. The optimal stopping problem is defined as monotone if $\forall n \ge 0 : A_n \subset A_{n+1}$, in other words, if at some stage n the loss function is not higher than the expected loss at the next stage, then this will be true for all future stages as well. In the terminology of anytime algorithms, the corresponding, though stronger, requirement is one of diminishing returns, which assumes that the improvement in quality is largest at the early stages of the process and diminishes over time [40].

Using backwards induction it can be proven that for the monotone stopping problems an optimal stopping rule has the following form:

$$N_{1-sla} = \min\big\{n \ge 0 : L_n \le \mathrm{E}_n(L_{n+1})\big\}. \qquad (11)$$

The rule N_{1-sla} (11) stops at the earliest stage when the current loss becomes less or equal to the expected loss at the next stage. It is called a "1-stage look-ahead" rule, or a "myopic" rule. With the loss function (1) the myopic rule takes the following form:

$$N_{1-sla} = \min\big\{n \ge 0 : \epsilon(R_n, \theta) - \mathrm{E}_n(\epsilon(R_{n+1}, \theta)) \le \\ \le \mathrm{E}_n(c_{n+1}) - c_n\big\}. \qquad (12)$$

For the case of monotone stopping problems where the error term of the loss function (1) is expressed as a distance ρ from an obtained result to the ground truth, i.e. $\epsilon(R_n, \theta) = \rho(R_n, R^*(\theta))$, in the paper [37] an approximation of the myopic rule (11) is proposed. Instead of estimating the difference between the current error and the expected error at the next stage it is proposed to estimate the expected distance between the current result to the result which would be obtained on the next stage. By means of triangle inequality, the left-hand side of the inequality in (12) is bounded by this value. Thus, an alternative stopping rule is obtained:

$$N_\Delta = \min\big\{n \ge 0 : \mathrm{E}_n(\rho(R_n, R_{n+1})) \le \\ \le \mathrm{E}_n(c_{n+1}) - c_n\big\}. \qquad (13)$$

As an approach for solving the optimal stopping problem (6) with an error term in the loss function L_n (1) expressed as an approximation error RSRE (8) of the ground truth image $R^*(\theta)$ by the partial reconstruction result R_n let us use a variant of the stopping rule N_Δ (13) under the following assumption:

Hypothesis 2 (H2) The distances between two consecutive tomographical reconstruction results in terms of the ℓ_2 metric decrease over time.

Using triangle inequality it can be shown that under the hypothesis H2 at the stage when the stopping conditions for the rule (13) are satisfied, the stopping problem becomes monotone starting from this stage and it is optimal to stop [37]. The rule (13) then takes the following form:

$$N_\Delta^{\mathrm{RSRE}} = \min\big\{n \ge 0 : \mathrm{E}_n(\|R_n - R_{n+1}\|_2) \le \\ \le \mathrm{E}_n(c_{n+1}) - c_n\big\}. \qquad (14)$$

In the cases of NRSRE (9) and S-RSRE (10) the stopping rule (14) can be used under the same hypothesis H2, however, the expression on the right hand side of the inequality needs to be multiplied by $\|R^*(\theta)\|_2$ and $S(R^*(\theta))$ respectively. Since from the perspective of a stopping rule the best approximation of the ground truth is the reconstruction result R_T on the last stage, the stopping rules for the error functions NRSRE (9) and S-RSRE (10) can be expressed as follows:

$$N_\Delta^{\mathrm{NRSRE}} = \min\big\{n \ge 0 : \mathrm{E}_n(\|R_n - R_{n+1}\|_2) \le \\ \le \|R_T\|_2 \cdot (\mathrm{E}_n(c_{n+1}) - c_n)\big\}, \qquad (15)$$

$$N_\Delta^{\text{S-RSRE}} = \min\big\{n \ge 0 : \mathrm{E}_n(\|R_n - R_{n+1}\|_2) \le \\ \le S(R_T) \cdot (\mathrm{E}_n(c_{n+1}) - c_n)\big\}. \qquad (16)$$

F. IMPLEMENTING THE STOPPING RULES

In the monitored reconstruction process on each stage n we acquire an additional projection (or several projections) and obtain a partial reconstruction result R_n. In order to apply the stopping rules constructed in the previous subsection, the following values need to be estimated:

1) The expected distance $\mathrm{E}_n(\|R_n - R_{n+1}\|_2)$ between the current reconstruction result and the next one.
2) The expected value $\mathrm{E}_n(c_{n+1})$ of the cost function on the next stage of the process.
3) For implementation of the stopping rule (15), the ℓ_2-norm of the last reconstruction result $\|R_T\|_2$.
4) For implementation of the stopping rule (16), the value of the Radon invariant $S(R_T)$, which can be calculated by analyzing the obtained projections $x_1, x_2, \dots, x_n$.

The method of modelling of the next result introduced in [37] is not applicable for the case of tomography (as the assumption of the next projection x_{n+1} having the same value as one of the previously acquired will lead to the same reconstruction result), thus in order to estimate the expected distance $\mathrm{E}_n(\|R_n - R_{n+1}\|_2)$ other methods should be used, such as methods of time series forecasting. We used the most basic estimation method where the target expected distance

This article has been accepted for publication in a future issue of this journal, but has not been fully edited. Content may change prior to final publication. Citation information: DOI 10.1109/ACCESS.2020.3002019, IEEE Access

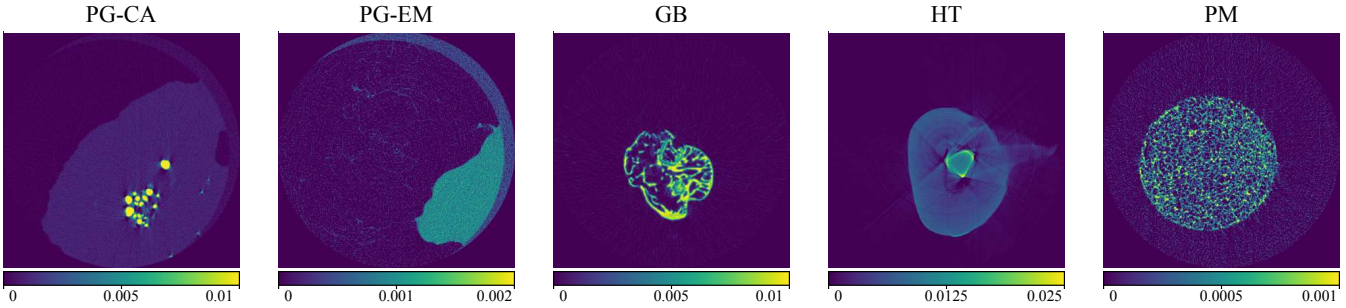

a) Pineal gland, section with calcification
b) Pineal gland, section without calcification
c) Gerbil bone
d) Human tooth with lead filling
e) Polylactide matrix

FIGURE 3. Reconstruction results for the evaluated objects. Values are given in px^{-1}, without normalization to the pixel size of the detector.

is assumed to be close to the distance between the two most recently obtained results:

$$\mathrm{E}_n(\|R_n - R_{n+1}\|_2) \approx \|R_{n-1} - R_n\|_2. \tag{17}$$

The method of estimating the expected cost function on the next stage inevitably depends on the cost structure. In the performed experiments we assumed the "anydose" algorithm model: each batch of acquired projections imparts a fixed dose $c > 0$, the exposure between projections is negligible, the time required to perform reconstruction is disregarded, and the cost function is proportional to the number of acquired projections (7). In this model, the difference between the expected cost function value on the next process stage and the current cost function simply equals the constant c:

$$\mathrm{E}_n(c_{n+1}) - c_n = c. \tag{18}$$

In order to implement the stopping rule $N_\Delta^{\mathrm{NRSRE}}$ (15) we assumed the following dependence model between the reconstruction result norm and the stage number n:

$$\|R_n\|_2 \approx \frac{a_0}{a_1 + n} + a_2. \tag{19}$$

The model parameters a_0, a_1, and a_2 of the regression (19) were determined at each stage n using the observed norms $\|R_1\|_2, \|R_2\|_2, \dots, \|R_n\|_2$ of the available reconstruction results in the following way: we used a ternary search through the values of a_1 on the outer level, then with a fixed value of a_1 the values of a_0 and a_2 were determined using a simple linear least squares fitting. Using the found parameters on each stage we extrapolated the value of $\|R_T\|_2$.

Finally, to implement the stopping rule $N_\Delta^{\text{S-RSRE}}$ (16) the Radon invariant $S(R_T)$ needs to be estimated. Its value does not differ significantly from the values $S(R_1), S(R_2), \dots, S(R_n)$ and from the sums of elements in each projection $S(x_1), S(x_2), \dots, S(x_n)$. To reduce the noise, all currently available projections may be used to calculate it:

$$S(R_T) \approx \frac{1}{n}\sum_{i=1}^{n} S(x_i). \tag{20}$$

With the established framework we can now proceed to test our hypotheses and evaluate the monitored tomographic reconstruction process.

III. EXPERIMENTAL EVALUATION

In this section we present the monitored reconstruction model evaluation on tomographic data obtained using laboratory microtomography setup in FSRC "Crystallography and photonics" of the Russian academy of sciences [55].

The experimental section is organized as follows: subsection III-A provides information about the evaluated objects, their 2D sections, and the tomographic measurement parameters, subsection III-B is dedicated to the evaluation of partial reconstruction errors and testing hypotheses H1 and H2, and subsection III-C contains the evaluation results for the implemented stopping rules.

A. EVALUATED OBJECTS

For experimental evaluation of the monitored tomographic reconstruction model described in Section II we used five 2D sections of different objects, obtained using the same laboratory X-ray tomography setup. Description of the evaluated objects, their sections, and published works related to the published imaging data, is presented in Table 1.

In the published materials the sinograms are obtained using the same X-ray laboratory microtomography setup developed in FSRC "Crystallography and Photonics" RAS, with a high voltage source GE ISOVOLT 3003, X-ray tube with molybdenum anode and XIMEA-xiRay 11Mpix X-ray detector with pixel size $9\mu\mathrm{m}$. There were no absorption filters between the X-ray source and the object. All tomographic projections of all samples were obtained with $20\mathrm{mA}$ current and $40\mathrm{kV}$ voltage setting. The experimental characteristics which differed between the objects are listed in Table 2. For all object sections, only the central square regions with size 1024×1024 px were evaluated. Reconstruction was performed using FBP method implemented in scikit-image 0.16.2 [56]. Reconstructed images for the evaluated 2D sections are presented in Figure 3.

This article has been accepted for publication in a future issue of this journal, but has not been fully edited. Content may change prior to final publication. Citation information: DOI 10.1109/ACCESS.2020.3002019, IEEE Access

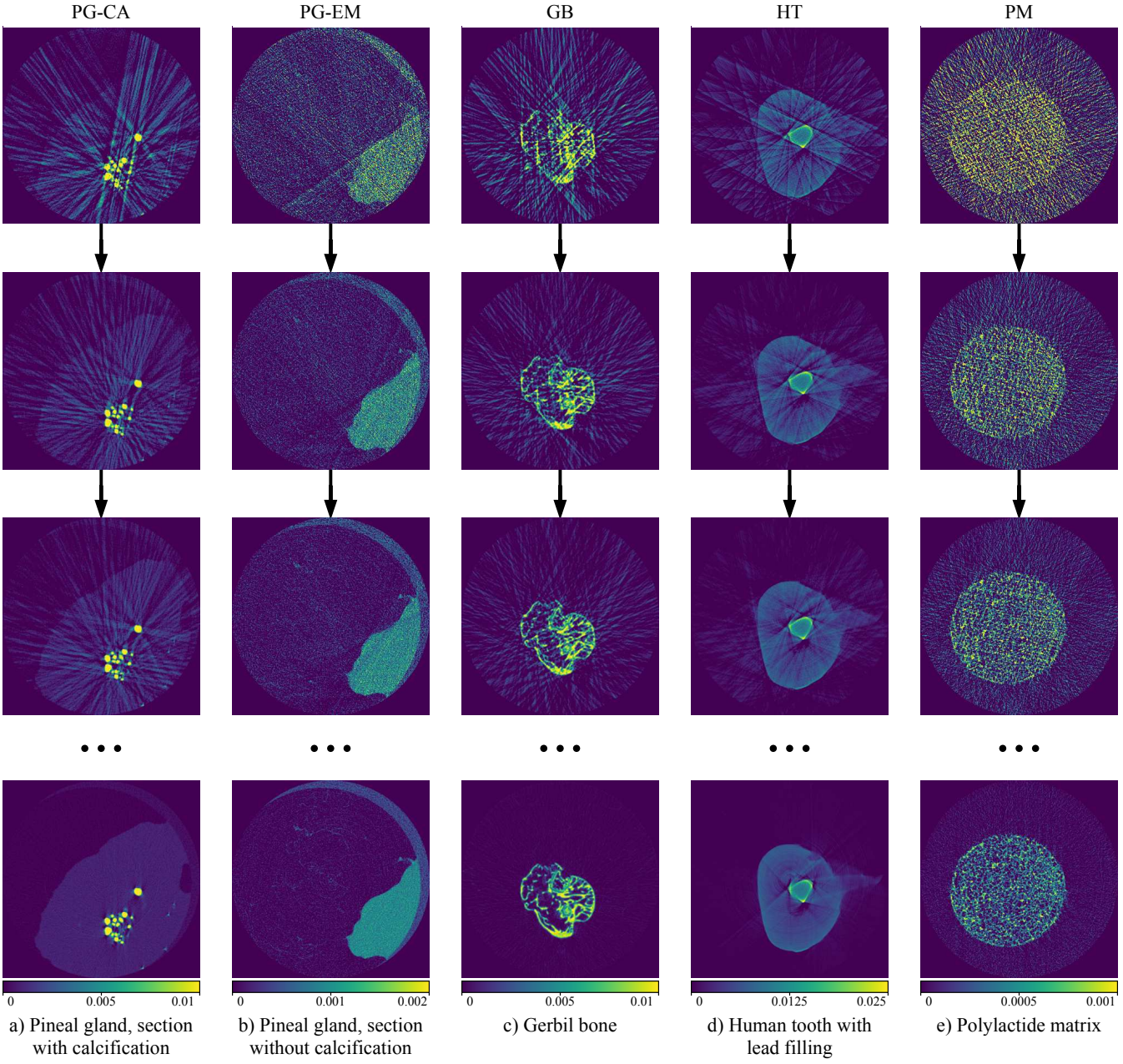

FIGURE 4. Examples of partial reconstructions for each object, with 20, 60, and 100 randomly drawn projections, with full reconstruction results given at the bottom for reference. Values are given in px^{-1}, without normalization to the pixel size of the detector.

TABLE 1. Objects used in the performed experiments

Object code	Description
PG-CA	Human pineal gland, section with visible calcification [57]
PG-EM	Human pineal gland, section without calcification [57]
GB	Gerbil bone section [58]
HT	Human tooth section with lead filling [55]
PM	Polylactide matrix section [59]

TABLE 2. Differences in experimental characteristics for different objects

Characteristic	PG-CA	PG-EM	GB	HT	PM
Emitter-object dist.	1.3m	1.3m	1.2m	1.2m	1.2m
Object-detector dist.	0.02m	0.02m	0.05m	0.05m	0.05m
Exposition	10s	10s	5s	5s	2.5s
Num. of projections	400	400	400	400	2000
Angular step	0.5°	0.5°	0.5°	0.5°	0.1°

This article has been accepted for publication in a future issue of this journal, but has not been fully edited. Content may change prior to final publication. Citation information: DOI 10.1109/ACCESS.2020.3002019, IEEE Access

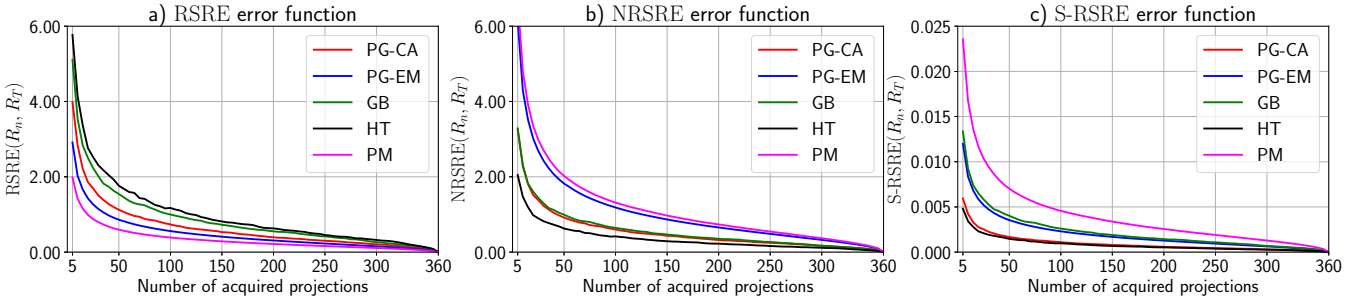

FIGURE 5. Convergence of the partial reconstruction results R_n to the last result R_T in terms of the error functions RSRE (8), NRSRE (9), and S-RSRE (10).

TABLE 3. Error function values for the partial reconstruction results of the evaluated objects with 50, 150, 250, and 350 projection angles.

Object code	RSRE (8)				NRSRE (9)				S-RSRE (10)			
	50 ang.	150 ang.	250 ang.	350 ang.	50 ang.	150 ang.	250 ang.	350 ang.	50 ang.	150 ang.	250 ang.	350 ang.
PG-CA	1.1240	0.5309	0.3023	0.0807	0.9175	0.4334	0.2468	0.0658	0.0017	0.0008	0.0005	0.0001
PG-EM	0.8594	0.4094	0.2287	0.0580	1.8198	0.8669	0.4844	0.1229	0.0035	0.0017	0.0009	0.0002
GB	1.5421	0.7257	0.4168	0.1101	0.9922	0.4670	0.2682	0.0709	0.0040	0.0019	0.0011	0.0003
HT	1.7632	0.8143	0.4529	0.1178	0.6263	0.2892	0.1609	0.0419	0.0015	0.0007	0.0004	0.0001
PM	0.5955	0.2858	0.1609	0.0405	2.0225	0.9705	0.5463	0.1375	0.0070	0.0034	0.0019	0.0005

B. EVALUATING PARTIAL RECONSTRUCTIONS

For each object we selected 360 projections in the angular range $[0°, 180°)$ with the angular step of $0.5°$, sampled at random without repetitions. The sequence of projections is constructed once for each evaluated object and is used in all further experiments with this object. Partial reconstructions were performed after adding five projections at a time from the sampled sequence. The random projection collection protocol allows to demonstrate the monitored reconstruction effects more clearly, while still remaining realistic. For example, such a sampling protocol could be supported with electron beam computed tomography (EBCT) set-ups [60].

After taking the next five projection the partial reconstruction was performed using the FBP method. Examples of partial reconstructions are presented in Figure 4.

In order to measure the effectiveness of the constructed stopping rules in a monitored reconstruction process setting we regarded the last reconstruction results R_T (presented in Figure 3), obtained using 360 projections, as the ground truth images for each object. Thus, the zero value of each evaluated error function corresponds to the full reconstruction, the best possible with a given measurement protocol.

Figure 5 illustrates the convergence of the partial reconstruction results to the last reconstruction result R_T if the functions RSRE (8), NRSRE (9), and S-RSRE (10) are used to represent the error function $\epsilon(R_n, \theta)$. It is clear that for each error function the convergence speed is different for different objects, the grouping of the objects by the convergence speed is different for each error function, and no grouping corresponds to the specific experimental characteristics presented in Table 2. This data supports the hypothesis H1, that the decrease speed of the error depends on the object, at least for the error functions evaluated in the scope of this paper. Error function values for the partial reconstruction results, corresponding to the plots in Figure 5 are presented in Table 3.

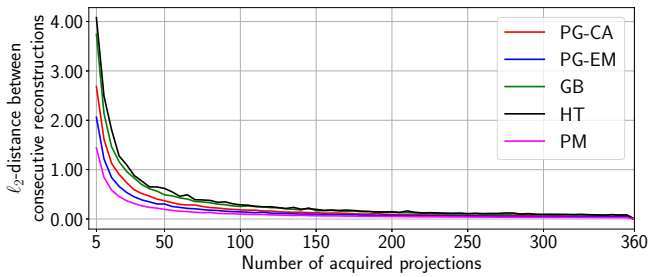

FIGURE 6. ℓ_2-distances between consecutive partial reconstruction results as the number of acquired projections increases.

TABLE 4. ℓ_2-distances between partial reconstruction result and the reconstruction result on the next stage (each stage adds 5 projection angles).

Object code	Number of projection angles						
	50	100	150	200	250	300	350
PG-CA	0.3689	0.1864	0.1282	0.0922	0.0785	0.0618	0.0602
PG-EM	0.3039	0.1454	0.0954	0.0719	0.0574	0.0473	0.0412
GB	0.4897	0.2552	0.1674	0.1427	0.1028	0.0895	0.0778
HT	0.6188	0.2864	0.1953	0.1448	0.1095	0.0944	0.0815
PM	0.1954	0.1000	0.0665	0.0510	0.0404	0.0340	0.0287

To check the hypothesis H2, which is necessary to apply the stopping rules (14), (15), and (16), derived in subsection II-E, we need to confirm that the ℓ_2-distances between consecutive partial reconstruction results decrease as the number of acquired projections increases. The plotted distances between the consecutive reconstruction results for all

This article has been accepted for publication in a future issue of this journal, but has not been fully edited. Content may change prior to final publication. Citation information: DOI 10.1109/ACCESS.2020.3002019, IEEE Access

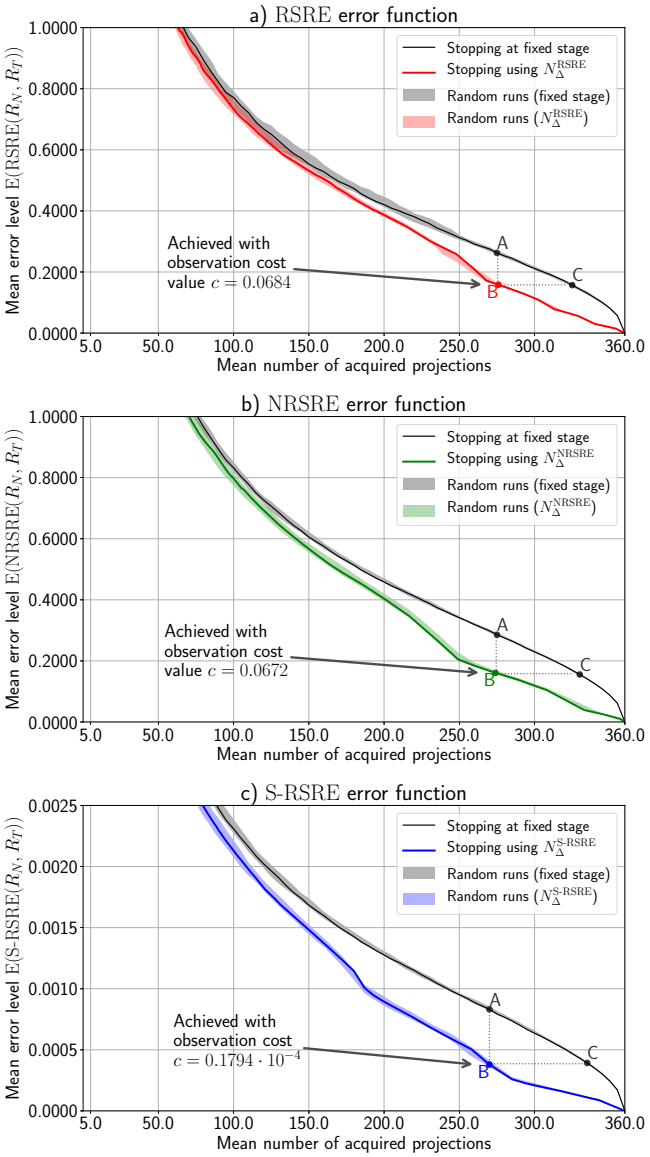

FIGURE 7. Expected performance profiles of the constructed stopping rules for the three evaluated error functions. Lower is better.

objects are presented in Figure 6, the corresponding distance values are presented in Table 4. We can observe a general decreasing trend in support of the hypothesis H2, although some discrepancies are present for object "HT", mostly when fewer projection angles are considered.

After the examination of the partial reconstruction results, we can proceed to evaluate the constructed stopping rules.

C. EVALUATING THE STOPPING RULES

The application of the stopping rules to the process of monitored tomographic reconstruction should allow achieving lower mean error level given a fixed mean number of acquired projections, or, respectively, the lower mean number of projections for the same mean error level. In order to evaluate and visualize that, it is convenient to analyze the expected performance profiles [40] of the stopping rules. Such performance profiles are obtained by plotting the mean error level (in our case it is expressed in terms of the error function $\epsilon(R_n, \theta)$ value averaged throughout the analyzed objects) of the partial reconstruction results against the mean number of projections acquired before the stopping condition is met, while varying the cost parameter c.

To provide a reference, in the same axes we can plot the mean error level achieved by reconstructing the objects with a fixed number of acquired projections. Such performance profile gives us a baseline stopping method – the one which always stops at a fixed stage, i.e. after a fixed pre-defined number of projections is acquired.

The expected performance profiles of the constructed stopping rules, alongside the baseline methods which stops at a fixed stage, are presented in Figure 7. Each point of the baseline plots is obtained by fixing the number of acquired projections and calculating the mean error function value for the reconstruction results of all objects. Each point of the stopping rule performance profile is obtained in a different way: with a fixed value of the observation cost c the monitored reconstruction was performed for each object, and the coordinates of the point were calculated by taking the mean number of acquired projections (averaged throughout the analyzed objects), and the corresponding mean error level achieved at stopping time.

Consider points A, B, and C on Figure 7a (corresponding to the experiment with RSRE error function (8)). Point A corresponds to the mean RSRE error level of 0.2627 which is achieved if for all objects we acquired and processed exactly 275 projection angles. Point B corresponds to the monitored reconstruction with the stopping rule N_Δ^{RSRE} (14) and observation cost value $c = 0.0684$. According to this stopping rule, the process stopped at different stages for different objects – namely, it stopped after 285 projections for the object "PG-CA", after 220 projections for "PG-EM", after 155 projections for the object "PM", and it never stopped for the objects "GB" and "HT" (which is to say that it stopped after 360 projections were obtained). As a result, the mean RSRE error level amounted to 0.1583. If all objects were to stop at the same stage, 325 projections had to be processed in order to achieve the same mean error level – on the baseline plot it corresponds to point C.

The coordinates of points A, B, and C presented on each subplot of Figure 7 along with the number of acquired projections and the reconstruction error level at stopping time for each object are presented in Table 5. Reconstruction results which correspond to the point B are presented in Figure 8.

It is evident that the performance profiles for the constructed stopping rules are positioned below the profiles of the baseline method for all evaluated error functions, which means that the stopping rules allow to achieve lower mean error levels with the same mean number of acquired projections (i.e. the same mean imparted dose) and, conversely, allow to obtain the reconstruction result with the same mean error level by taking fewer projections on average.

This article has been accepted for publication in a future issue of this journal, but has not been fully edited. Content may change prior to final publication. Citation information: DOI 10.1109/ACCESS.2020.3002019, IEEE Access

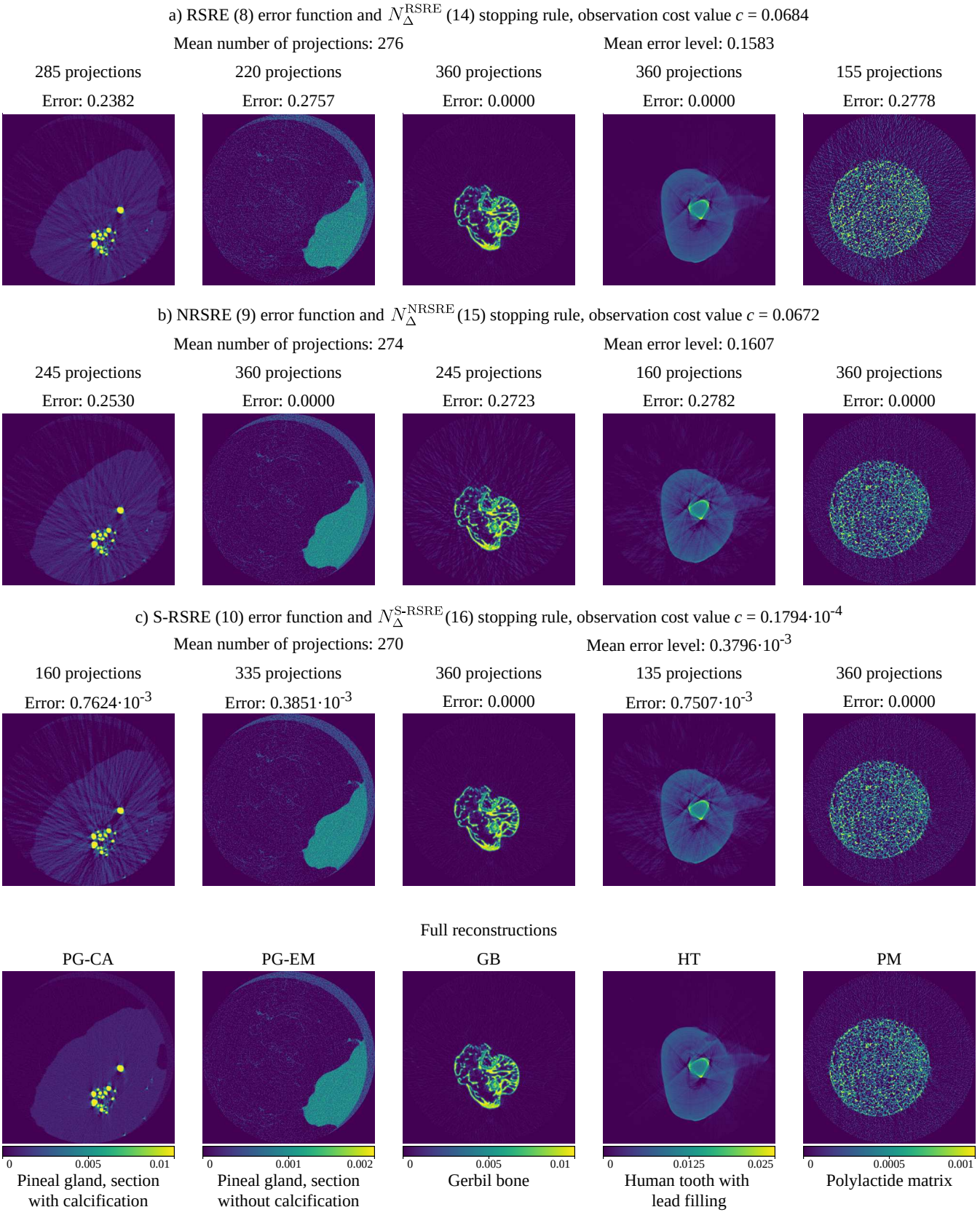

FIGURE 8. Reconstruction results achieved at stopping time for all objects, corresponding to the point B in Figure 7, for the three evaluated error functions and their corresponding stopping rules. Full reconstructions are given at the bottom for reference.

This article has been accepted for publication in a future issue of this journal, but has not been fully edited. Content may change prior to final publication. Citation information: DOI 10.1109/ACCESS.2020.3002019, IEEE Access

TABLE 5. Number of acquired projections and the error levels at stopping time for each object, corresponding to points A, B, and C in Figure 7.

a) RSRE (8) error function and $N_{\Delta}^{\mathrm{RSRE}}$ (14) stopping rule						
Object code	Point A		Point B		Point C	
	Angles	Error	Angles	Error	Angles	Error
PG-CA	275	0.2556	285	0.2382	325	0.1534
PG-EM	275	0.1909	220	0.2757	325	0.1120
GB	275	0.3416	360	0.0000	325	0.1984
HT	275	0.3911	360	0.0000	325	0.2418
PM	275	0.1342	155	0.2778	325	0.0794
Mean	275	0.2627	276	0.1583	325	0.1570

b) NRSRE (9) error function and $N_{\Delta}^{\mathrm{NRSRE}}$ (15) stopping rule						
Object code	Point A		Point B		Point C	
	Angles	Error	Angles	Error	Angles	Error
PG-CA	275	0.2086	245	0.2530	330	0.1176
PG-EM	275	0.4042	360	0.0000	330	0.2185
GB	275	0.2198	245	0.2723	330	0.1182
HT	275	0.1389	160	0.2782	330	0.0757
PM	275	0.4558	360	0.0000	330	0.2472
Mean	275	0.2855	274	0.1607	330	0.1554

c) S-RSRE (10) error function and $N_{\Delta}^{\text{S-RSRE}}$ (16) stopping rule Error levels are multiplied by 1000						
Object code	Point A		Point B		Point C	
	Angles	Error	Angles	Error	Angles	Error
PG-CA	270	0.3939	160	0.7624	335	0.1912
PG-EM	270	0.8170	335	0.3851	335	0.3851
GB	270	0.9545	360	0.0000	335	0.4477
HT	270	0.3383	135	0.7507	335	0.1586
PM	270	1.6543	360	0.0000	335	0.7794
Mean	270	0.8316	270	0.3796	335	0.3924

TABLE 6. Achieved mean values of error functions with restricted mean number of acquired projections. Lower is better.

a) RSRE (8) error function and $N_{\Delta}^{\mathrm{RSRE}}$ (14) stopping rule							
Stopping method	Limitation to the mean number of projection angles						
	≤ 50	≤ 100	≤ 150	≤ 200	≤ 250	≤ 300	≤ 350
Baseline	1.177	0.771	0.553	0.421	0.312	0.211	0.081
$N_{\Delta}^{\mathrm{RSRE}}$	1.153	0.739	0.544	0.399	0.259	0.128	0.024

b) NRSRE (9) error function and $N_{\Delta}^{\mathrm{NRSRE}}$ (15) stopping rule							
Stopping method	Limitation to the mean number of projection angles						
	≤ 50	≤ 100	≤ 150	≤ 200	≤ 250	≤ 300	≤ 350
Baseline	1.276	0.832	0.605	0.458	0.341	0.229	0.088
$N_{\Delta}^{\mathrm{NRSRE}}$	1.228	0.797	0.582	0.449	0.206	0.138	0.025

c) S-RSRE (10) error function and $N_{\Delta}^{\text{S-RSRE}}$ (16) stopping rule Error levels are multiplied by 1000							
Stopping method	Limitation to the mean number of projection angles						
	≤ 50	≤ 100	≤ 150	≤ 200	≤ 250	≤ 300	≤ 350
Baseline	3.543	2.309	1.684	1.276	0.951	0.635	0.244
$N_{\Delta}^{\text{S-RSRE}}$	3.367	2.162	1.504	0.893	0.595	0.226	0.087

In order to rule out the possibility that the observed effect depends on the random draw of projections, we repeated the experiment 25 times with different random projection orders. Color-filled areas in Figure 7 correspond to the areas occupied by the performance profiles obtained with different experimental runs. It can be seen that the actual random projections order does not significantly influence the respective positions of the performance profiles.

Table 6 shows the achieved mean error level (in terms of the evaluated error functions) at stopping time, using the constructed stopping methods, and with a restriction to the mean number of acquired projections, which corresponds to a restricted mean dose. The mean error values presented in Table 6 correspond to points of the stopping method's performance profile which yield the closest mean number of acquired projections without exceeding the limitation. It can be observed, that the application of the stopping rule allows to achieve lower mean reconstruction error levels than the baseline for each evaluated error function and for each restriction level.

The selection of the error function for the reconstruction result may depend significantly on the practical application and setup. As it was shown in subsection II-E, the construction of the stopping rule requires for the structure of the error function to be known, and if other quality metrics are used, the appropriate stopping rules should be specifically constructed for them. However, for some quality metrics, the stopping rules derived in this paper could provide good results without modification. For example, if the structural similarity metric SSIM [48] is used, the stopping rule $N_{\Delta}^{\mathrm{RSRE}}$ (14) outperforms stopping at a fixed stage (see Figure 9 and Table 7), presumably due to a correlation between SSIM and RSRE (8) on the analyzed dataset. As with Figure 7, the color-filled areas in Figure 9 correspond to the areas occupied by the performance profiles obtained with 25 experimental runs with different random order of projections. For calculation of SSIM metric we used its implementation in scikit-image 0.16.2 [56] with default parameters and data range length of 1.0 for reconstructed images with floating-point data type.

IV. DISCUSSION

For the evaluation of a monitored tomographic reconstruction process in an "anydose" model, we used five sinograms of object sections, collected with the laboratory X-ray tomography set-up in a parallel scheme. Partial reconstructions were performed in stages, where on each stage five new random projections were drawn from the sinogram and were used to update the reconstructed image. Figure 5 illustrates the dynamics of the reconstruction error level, calculated in three different ways, with regards to the process stage. Since the main experimental parameters (projections collection protocol, tube current, anode type, detector, etc.) were the same, the differences in the error level curves signify the dependence of the dynamic error behaviour on inherent properties of the probed object.

This article has been accepted for publication in a future issue of this journal, but has not been fully edited. Content may change prior to final publication. Citation information: DOI 10.1109/ACCESS.2020.3002019, IEEE Access

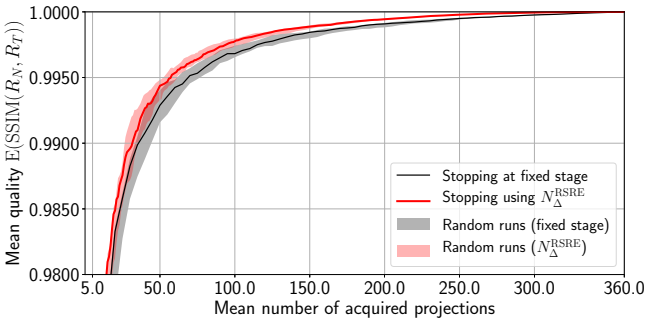

FIGURE 9. Expected performance profile of the stopping rule N_Δ^{RSRE} with SSIM quality metric [48] for the evaluated objects. Higher is better.

TABLE 7. Achieved mean values of SSIM quality metric with restricted mean number of projections using the stopping rule N_Δ^{RSRE}. Higher is better.

Stopping method	Limitation to the mean number of projections						
	≤ 50	≤ 100	≤ 150	≤ 200	≤ 250	≤ 300	≤ 350
Baseline	0.9929	0.9968	0.9984	0.9991	0.9995	0.9998	1.0000
N_Δ^{RSRE}	0.9944	0.9977	0.9988	0.9994	0.9998	0.9999	1.0000

It is worth to note that the ordering of plots in Figure 5 by the speed of the error decrease given a fixed experimental setup and error function is interesting in itself, as it suggests a method of objects classification by some inherent properties. The identification of properties of probed objects which influence the rate of error decrease and investigating the ways of using this information to enhance the reconstruction quality or speed could be a subject for future studies with a larger dataset of sample objects.

Figure 6 shows the decrease of ℓ_2-distances between consecutive partial reconstruction results from stage to stage. This decrease (referred to in the hypothesis H2) is required in order for the constructed stopping rules to be consistent: since these distances are thresholded in the stopping rules, their decrease guarantees that if the stopping condition is met, it will be met at the future stages as well (and thus it is reasonable to stop at the current stage). Deviations from the decreasing trend will impact the stopping rules as follows: minor discrepancies, which lead to the observed distance being higher than expected, such as the ones seen for the object "HT" in Figure 6, may lead to a delayed stopping. However, if the measured distance will deviate in the other direction (i.e. will be lower than expected), it could lead to preliminary stopping before the desired reconstruction quality is reached. This could be mitigated by increasing the number of projections added at each stage of the process.

Figure 7 illustrates the averaged experimental profiles of two types: reconstruction with stopping at a fixed stage (that is, after a fixed number of projections is collected), and with stopping using the constructed rules (14)–(16). The presented results confirm that the monitored reconstruction approach in an "anydose" model allows to reduce the mean reconstruction error with a given mean number of analyzed projections.

The primary goal of this paper was to demonstrate the concept of a monitored reconstruction and an impact of applying stopping rules to the tomographic imaging process. For this reason the experiments in Section III were conducted on 2D sections. However, the monitored reconstruction framework presented in Section II is applicable for a full 3D reconstruction as well, and the evaluation of stopping rules for 3D reconstruction should be a subject of future work. Moreover, even the results in 2D could be relevant for practical applications, as it might be feasible to make a stopping decision for 3D reconstruction by analyzing partial reconstructions of one or several central sections [52].

In order to demonstrate the effect of the stopping rules, which allow to dynamically adjust the number of used projections, in the performed experiments we used the full reconstruction results as the ground truth. The usage of actual ground truth for the objects, which could be achieved in simulation studies or physical phantom studies, would help to account for both components of the true error (the one related to the reconstruction algorithm and measurement parameters, and the one related to the number of used projections), however the stopping rules only influence the second component. Essentially, the full reconstruction results *are* the ground truth for the stopping problem, as the "good" reconstruction result might not even be achievable due to the problems with the scanning protocol, or measurement configuration. With a traditional tomographic scanning process such problems would be detected only after all projections were collected, and the object was imparted with a full dose, whereas the monitored reconstruction should be able to detect that the current partial reconstruction result will not become any better, and stop the process before all projections are collected. Thus, the stopping rules should be designed to terminate the process when the partial reconstructions stop significantly changing, i.e. when their become close to the "final" reconstruction result. Nevertheless, for implementing the monitored reconstruction process in a practical setting, additional research should be performed with regards to the absolute impact of the two error components.

One of the limitations of the monitored reconstruction approach is the dependence on the protocol for acquiring projections, as it is required for the partial reconstructions to produce meaningful results, improving over time according to a selected metric function. The random projections sampling evaluated in Section III conforms to this requirement, but may constrain the practical implementation. In the scope of future work it is planned to evaluate different sampling protocols, such as uniform sampling with variable angular offset, and perform a comparison of approaches with different protocols, e.g. monitored reconstruction with random sampling against a regular reconstruction with a fixed number of uniformly drawn projections.

A major disadvantage of the monitored reconstruction process is the need to perform partial reconstructions in order to estimate the change of the error level on the next stage and implement the stopping rule. For an "anydose" model the extra computational cost associated with partial

reconstructions is less relevant, as the main target of such model is the reduction of the number of X-ray projections, however it is relevant if scanning time or reconstruction time is an important factor contributing to the observation cost function (1). While for integral reconstruction methods such as FBP the partial reconstructions could be updated after obtaining new projection angles, in order to achieve the same for the iterative methods, some special techniques should be designed and implemented.

V. CONCLUSION

In this paper, we introduced a monitored reconstruction process, a novel approach to the tomographic reconstruction which allows to consider it as an anytime algorithm. In a monitored reconstruction process, partial reconstruction results are generated after several projections are obtained, and based on the differences between the consequent partial reconstruction results, the stopping decision is made. It was shown that stopping rules can be constructed which would allow to achieve lower mean reconstruction error level given the same mean number of collected projections, and vice versa, the same mean reconstruction error could be obtained using fewer projections on average, due to stopping at different times for different scanned objects.

As future work we plan to expand the number of used reconstruction error metrics, to include analysis of local geometric properties, boundaries, and spatial anisotropy, evaluate different projection collection protocols to broaden the potential scope of usage, and explore the modifications to the tomographic reconstruction algorithms necessary to speed up the partial reconstruction results generation.

ACKNOWLEDGMENT

Authors are grateful to the Federal Scientific Research Center "Crystallography and Photonics" of the Russian Academy of Sciences for the X-ray tomography measurements.

REFERENCES

[1] A. C. Kak and M. Slaney, Principles of Computerized Tomographic Imaging, ser. Classics in Applied Mathematics. Society for Industrial and Applied Mathematics, Philadelphia, USA, 2001, DOI: 10.1137/1.9780898719277.

[2] T. Buzug, Computed Tomography. Springer-Verlag, Berlin, Heidelberg, 2008, DOI: 10.1007/978-3-540-39408-2.

[3] E. Topal, Z. Liao, M. Löffler, J. Gluch, J. Zhang, X. Feng, and E. Zschech, "Multi-scale X-ray tomography and machine learning algorithms to study MoNi4 electrocatalysts anchored on MoO2 cuboids aligned on Ni foam," BMC Materials, no. 2, 2020, Art. ID 5, DOI: 10.1186/s42833-020-00011-0.

[4] M. Polikarpov, G. Bourenkov, I. Snigireva, A. Snigirev, S. Zimmermann, K. Csanko, S. Brockhauser, and T. R. Schneider, "Visualization of protein crystals by high-energy phase-contrast X-ray imaging," Acta Crystallographica Section D, vol. 75, no. 11, pp. 947–958, 2019, DOI: 10.1107/S2059798319011379.

[5] M. Sokac, I. Budak, M. Katic, Z. Jakovljevic, Z. Santosi, and D. Vukelic, "Improved surface extraction of multi-material components for single-source industrial X-ray computed tomography," Measurement, vol. 153, 2020, Art. ID 107438, DOI: 10.1016/j.measurement.2019.107438.

[6] P. Hermanek, F. Zanini, and S. Carmignato, "Traceable Porosity Measurements in Industrial Components Using X-Ray Computed Tomography," J. of Manufacturing Sci. and Eng., vol. 141, no. 5, 2019, Art. ID 051004, DOI: 10.1115/1.4043192.

[7] M. Khoury, H. Li, P. Li, Y. C. Chow, B. Bonef, H. Zhang, M. S. Wong, S. Pinna, J. Song, J. Choi, J. S. Speck, S. Nakamura, and S. P. DenBaars, "Polarized monolithic white semipolar (20–21) InGaN light-emitting diodes grown on high quality (20–21) GaN/sapphire templates and its application to visible light communication," Nano Energy, vol. 67, 2020, Art. ID 104236, DOI: 10.1016/j.nanoen.2019.104236.

[8] K. J. Batenburg, S. Bals, J. Sijbers, C. Kübel, P. A. Midgley, J. C. Hernandez, U. Kaiser, E. R. Encina, E. A. Coronado, and G. V. Tendeloo, "3D imaging of nanomaterials by discrete tomography," Ultramicroscopy, vol. 109, no. 6, pp. 730–740, 2009, DOI: 10.1016/j.ultramic.2009.01.009.

[9] A. Pakhnevich, A. Kurkin, A. Lavrov, K. Tarasenko, E. Kovalenko, A. Kaloyan, and K. Podurets, "Synchrotron and Neutron Tomography of Paleontological Objects on the Facilities of the Kurchatov Institute," J. of Imaging, vol. 4, no. 8, 2018, Art. ID 103, DOI: 10.3390/jimaging4080103.

[10] I. Bukreeva, A. Mittone, A. Bravin, G. Festa, M. Alessandrelli, P. Coan, V. Formoso, R. G. Agostino, M. Giocondo, F. Ciuchi, M. Fratini, L. Massimi, A. Lamarra, C. Andreani, R. Bartolino, G. Gigli, G. Ranocchia, and A. Cedola, "Virtual unrolling and deciphering of Herculaneum papyri by X-ray phase-contrast tomography," Sci. Reports, vol. 6, 2016, Art. ID 27227, DOI: 10.1038/srep27227.

[11] X. Duan, J. Cheng, L. Zhang, Y. Xing, Z. Chen, and Z. Zhao, "X-ray cargo container inspection system with few-view projection imaging," Nuclear Instruments and Methods in Phys. Res. Section A, vol. 598, no. 2, pp. 439–444, 2009, DOI: 10.1016/j.nima.2008.08.151.

[12] N. Hättenschwiler, S. Merks, and A. Schwaninger, "Airport security x-ray screening of hold baggage: 2d versus 3d imaging and evaluation of an on-screen alarm resolution protocol," in Int. Carnahan Conf. on Security Tech. (ICCST), 2018, pp. 1–5, DOI: 10.1109/CCST.2018.8585713.

[13] B. Wildman-Tobriner, B. C. Allen, and C. M. Maxfield, "Common Resident Errors When Interpreting Computed Tomography of the Abdomen and Pelvis: A Review of Types, Pitfalls, and Strategies for Improvement," Current Problems in Diagnostic Radiology, vol. 48, no. 1, pp. 4–9, 2019, DOI: 10.1067/j.cpradiol.2017.12.010.

[14] Y. Kwong, A. O. Mel, G. Wheeler, and J. M. Troupis, "Four-dimensional computed tomography (4DCT): A review of the current status and applications," J. of Medical Imaging and Radiation Oncology, vol. 59, no. 5, pp. 545–554, 2015, DOI: 10.1111/1754-9485.12326.

[15] C.-H. Chien, F.-C. Shih, C.-Y. Chen, C.-H. Chen, W.-L. Wu, and C.-W. Mak, "Unenhanced multidetector computed tomography findings in acute central pulmonary embolism," BMC Medical Imaging, vol. 19, 2019, Art. ID 65, DOI: 10.1186/s12880-019-0364-y.

[16] N. Smelkina, A. Kolsanov, S. Chaplygin, P. Zelter, and A. Khramov, "Pulmonary Emphysema Recognition by CT scan," Computer Optics, vol. 41, no. 5, 2017, DOI: 10.18287/2412-6179-2017-41-5-726-731 (In Russian).

[17] K.-J. Yoo, D. Choi, B. W. Choi, S.-H. Lim, and B.-C. Chang, "The comparison of the graft patency after coronary artery bypass grafting using coronary angiography and multi-slice computed tomography," Europ. J. of Cardio-Thoracic Surgery, vol. 24, no. 1, pp. 86–91, 2003, DOI: 10.1016/S1010-7940(03)00192-1.

[18] D. R. Coles, M. A. Smail, I. S. Negus, P. Wilde, M. Oberhoff, K. R. Karsch, and A. Baumbach, "Comparison of Radiation Doses From Multislice Computed Tomography Coronary Angiography and Conventional Diagnostic Angiography," J. of the American College of Cardiology, vol. 47, no. 9, pp. 1840–1845, 2006, DOI: 10.1016/j.jacc.2005.11.078.

[19] I. Kuchin, T. Imaev, P. Lepilin, A. Kolegaev, I. Medvedeva, A. Komlev, S. Ternovoi, and R. Akchurin, "State of the art of the problem concerning endovascular treatment of abdominal aortic aneurysms of infrarenal localization," Angiol Sosud Khir, vol. 24, no. 3, pp. 60–65, 2018, (In Russian).

[20] A. E. Hughes, A. Trinchi, F. F. Chen, Y. S. Yang, I. S. Cole, S. Sellaiyan, J. Carr, P. D. Lee, G. E. Thompson, and T. Q. Xiao, "The application of multiscale quasi 4D CT to the study of SrCrO4 distributions and the development of porous networks in epoxy-based primer coatings," Progress in Organic Coatings, vol. 77, no. 11, pp. 1946–1956, 2014, DOI: 10.1016/j.porgcoat.2014.07.001.

[21] T. Suzuki, T. Shiotani, and M. Ohtsu, "Evaluation of cracking damage in freeze-thawed concrete using acoustic emission and X-ray CT image," Construction and Building Materials, vol. 136, pp. 619–626, 2017, DOI: 10.1016/j.conbuildmat.2016.09.013.

[22] Y. Wang, R. Song, J.-J. Liu, M.-M. Cui, and P. G. Ranjith, "Pore scale investigation on scaling-up micro-macro capillary number and wettability on trapping and mobilization of residual fluid," J. of Contaminant Hydrology, vol. 225, 2019, Art. ID 103499, DOI: 10.1016/j.jconhyd.2019.103499.

[23] T. dos Santos Rolo, A. Ershov, T. van de Kamp, and T. Baumbach, "In vivo X-ray cine-tomography for tracking morphological dynamics," Proc.

of the National Academy of Sci., vol. 111, no. 11, pp. 3921–3926, 2014, DOI: 10.1073/pnas.1308650111.

[24] S. E. Adamczak, F. J. Bova, and D. J. Hoh, "Intraoperative 3D Computed Tomography: Spine Surgery," Neurosurgery Clinics of North America, vol. 28, no. 4, pp. 585–594, 2017, DOI: 10.1016/j.nec.2017.06.002.

[25] H. Villarraga-Gómez, C. Peitsch, A. Ramsey, and S. Smith, "The Role of Computed Tomography in Additive Manufacturing," in ASPE and euspen Summer Topical Meeting: Advancing Precision in Additive Manufacturing, 2018, pp. 201–210.

[26] J. Z. Liang, P. J. La Riviere, G. El Fakhri, S. J. Glick, and J. Siewerdsen, "Guest Editorial Low-Dose CT: What Has Been Done, and What Challenges Remain?" IEEE Trans. on Med. Imag., vol. 36, no. 12, pp. 2409–2416, 2017, DOI: 10.1109/TMI.2017.2768978.

[27] M. K. Kalra, M. M. Maher, T. L. Toth, L. M. Hamberg, M. A. Blake, J.-A. Shepard, and S. Saini, "Strategies for CT Radiation Dose Optimization," Radiology, vol. 230, no. 3, pp. 619–628, 2004, DOI: 10.1148/radiol.2303021726.

[28] T. L. Slovis, "The ALARA Concept in Pediatric CT: Myth or Reality?" Radiology, vol. 223, no. 1, pp. 5–6, 2002, DOI: 10.1148/radiol.2231012100.

[29] A. Sabarudin and Z. Sun, "Radiation dose measurements in coronary CT angiography," World J. of Cardiology, vol. 5, no. 12, pp. 459–464, 2013, DOI: 10.4330/wjc.v5.i12.459.

[30] M. F. McNitt-Gray, "AAPM/RSNA Physics Tutorial for Residents: Topics in CT," RadioGraphics, vol. 22, no. 6, pp. 1541–1553, 2002, DOI: 10.1148/rg.226025128.

[31] N. Irnstorfer, E. Unger, A. Hojreh, and P. Homolka, "An anthropomorphic phantom representing a prematurely born neonate for digital x-ray imaging using 3D printing: Proof of concept and comparison of image quality from different systems," Sci. Reports, vol. 9, no. 1, 2019, Art. ID 14357, DOI: 10.1038/s41598-019-50925-3.

[32] K. MacGregor, I. Li, T. Dowdell, and B. G. Gray, "Identifying Institutional Diagnostic Reference Levels for CT with Radiation Dose Index Monitoring Software," Radiology, vol. 276, no. 2, pp. 507–517, 2015, DOI: 10.1148/radiol.2015141520.

[33] G. Wang, H. Yu, and Y. Ye, "A scheme for multisource interior tomography," Med. Phys., vol. 36, no. 8, pp. 3575–3581, 2009, DOI: 10.1118/1.3157103.

[34] T. K. Mittal and M. B. Rubens, Computed Tomography Techniques and Principles. Part a. Electron Beam Computed Tomography. London: Springer London, 2006, pp. 93–98, DOI: 10.1007/1-84628-156-3_6.

[35] W. Yang, H. Zhang, J. Yang, J. Wu, X. Yin, Y. Chen, H. Shu, L. Luo, G. Coatrieux, Z. Gui, and Q. Feng, "Improving Low-Dose CT Image Using Residual Convolutional Network," IEEE Access, vol. 5, pp. 24 698–24 705, 2017, DOI: 10.1109/ACCESS.2017.2766438.

[36] M. C. Horsch and D. Poole, "An anytime algorithm for decision making under uncertainty," in Proc. of the 14th Conf. on Uncertainty in Artificial Intelligence, ser. UAI'98. San Francisco, CA, USA: Morgan Kaufmann Publishers Inc., 1998, pp. 246–255.

[37] K. Bulatov, N. Razumnyi, and V. V. Arlazarov, "On optimal stopping strategies for text recognition in a video stream as an application of a monotone sequential decision model," Int. J. on Document Analysis and Recognit., vol. 22, no. 3, pp. 303–314, 2019, DOI: 10.1007/s10032-019-00333-0.

[38] K. Bulatov, B. Savelyev, and V. V. Arlazarov, "Next integrated result modelling for stopping the text field recognition process in a video using a result model with per-character alternatives," in 12th Int. Conf. on Machine Vision (ICMV, vol. 11433. SPIE, 2020, pp. 710–716, DOI: 10.1117/12.2559447.

[39] T. Chernov, N. Razumnuy, A. Kozharinov, D. Nikolaev, and V. Arlazarov, "Image quality assessment for video stream recognition systems," J. of Informat. Tech. and Comput. Sys., vol. 4, pp. 71–82, 2017, (In Russian).

[40] S. Zilberstein, "Using anytime algorithms in intelligent systems," AI Magazine, vol. 17, no. 3, pp. 73–83, 1996, DOI: 10.1609/aimag.v17i3.1232.

[41] T. Ferguson, Mathematical statistics: a decision theoretic approach, ser. Probability and mathematical statistics. Academic Press, 1967.

[42] T. S. Ferguson, "Optimal stopping and applications," 2008. [Online]. Available: {https://www.math.ucla.edu/~tom/Stopping}

[43] S. Basu and Y. Bresler, "$O(N^2 \log_2 N)$ filtered backprojection reconstruction algorithm for tomography," IEEE Trans. on Image Process., vol. 9, no. 10, pp. 1760–1773, 2000, DOI: 10.1109/83.869187.

[44] M. Beister, D. Kolditz, and W. A. Kalender, "Iterative reconstruction methods in X-ray CT," Physica Medica, vol. 28, no. 2, pp. 94–108, 2012, DOI: 10.1016/j.ejmp.2012.01.003.

[45] K. Bulatov, M. Chukalina, and D. Nikolaev, "Fast X-Ray Sum Calculation Algorithm for Computed Tomography Problem," Bull. of the South Ural State Univ. Ser. Math. Modelling, Programming & Comp. Software, vol. 13, no. 1, pp. 95–106, 2020, DOI: 10.14529/mmp200107.

[46] E. A. Cheremukhin and A. I. Chulichkov, "On the application of computer measurement systems in tomography," Comput. Math. and Math. Phys., vol. 45, no. 4, pp. 716–726, 2005, (In Russian).

[47] L. W. Goldman, "Principles of CT: Radiation Dose and Image Quality," J. of Nuclear Medicine Tech., vol. 35, no. 4, pp. 213–225, 2007, DOI: 10.2967/jnmt.106.037846.

[48] Zhou Wang, A. C. Bovik, H. R. Sheikh, and E. P. Simoncelli, "Image quality assessment: from error visibility to structural similarity," IEEE Transactions on Image Processing, vol. 13, no. 4, pp. 600–612, 2004, DOI: 10.1109/TIP.2003.819861.

[49] J. Wu, F. Qi, e. W. Shi, Guangming", D. Xu, A. Ho, J. Wu, Y. He, J. Cai, M. Kankanhalli, and M.-T. Sun, "Image quality assessment based on improved structural similarity," in Advances in Multimedia Information Processing – PCM 2012. Berlin, Heidelberg: Springer Berlin Heidelberg, 2012, pp. 153–163, DOI: 10.1007/978-3-642-34778-8_14.

[50] A. B. Watson, Q. J. Hu, and J. F. M. III, "Digital video quality metric based on human vision," Journal of Electronic Imaging, vol. 10, no. 1, pp. 20–29, 2001, DOI: 10.1117/1.1329896.

[51] H. Wang, Y. Zhou, S. Su, Z. Hu, J. Liao, and Y. Chang, "Adaptive Volterra Filter for Parallel MRI Reconstruction," EURASIP J. on Advances in Signal Process., vol. 34, 2019, DOI: 10.1186/s13634-019-0633-5.

[52] A. S. Ingacheva and M. V. Chukalina, "Polychromatic CT Data Improvement with One-Parameter Power Correction," Math. Problems in Eng., 2019, Art. ID 1405365, DOI: 10.1155/2019/1405365.

[53] B. A. Berezovskij and A. V. Gnedin, "Theory of choice and the problem of optimal stopping at the best entity." Autom. Remote Control, vol. 42, pp. 1221–1225, 1981.

[54] Y. S. Chow and H. Robbins, "A Martingale System Theorem and Applications," in Proc 4th Berkeley Symp Math Stat Probabilit, vol. 1. Berkeley, Calif.: Univ. of Calif. Press, 1961, pp. 93–104.

[55] A. V. Buzmakov, V. E. Asadchikov, D. A. Zolotov, B. S. Roshchin, Y. M. Dymshits, V. A. Shishkov, M. V. Chukalina, A. S. Ingacheva, D. E. Ichalova, Y. S. Krivonosov, I. G. Dyachkova, M. Balzer, M. Castele, S. Chilingaryan, and A. Kopmann, "Laboratory Microtomographs: Design and Data Processing Algorithms," Crystallography Reports, vol. 63, no. 6, pp. 1057–1061, 2018, DOI: 10.1134/S106377451806007X.

[56] S. van der Walt, J. L. Schönberger, J. Nunez-Iglesias, F. Boulogne, J. D. Warner, N. Yager, E. Gouillart, T. Yu, and the scikit-image contributors, "scikit-image: image processing in Python," PeerJ, vol. 2:e453, 2014, DOI: 10.7717/peerj.453.

[57] E. I. Fokin, S. V. Savel'ev, V. I. Gulimova, E. V. Asadchikov, R. A. Senin, and A. V. Buzmakov, "The morphogenesis and spatial organization of human pineal gland concretions in Alzheimer's disease, schizophrenia, and alcoholism," Archive of pathology, vol. 68, no. 5, pp. 20–22, 2006, (In Russian).

[58] V. Gulimova, A. Proshchina, A. Kharlamova, Y. Krivova, V. Barabanov, R. Berdiev, V. Asadchikov, A. Buzmakov, D. Zolotov, and S. Saveliev, "Reptiles in Space Missions: Results and Perspectives," Int. J. of Molecular Sci., vol. 20, no. 12, 2019, Art. ID 3019, DOI: 10.3390/ijms20123019.

[59] Y. Krivonosov, M. Chukalina, A. Buzmakov, V. Asadchikov, A. Rusakov, A. Mariyanats, V. Popov, I. Zanin, and V. Kulik, "Study of polylactide matrices using x-ray microtomography," Industrial laboratory, Diagnostics of materials, vol. 86, no. 1, pp. 26–31, 2020, DOI: 10.26896/1028-6861-2020-86-1-26-31 (In Russian).

[60] C.-J. Tan, C.-X. Tang, W.-H. Huang, Q.-X. Jin, Y.-C. Du, Q. Luo, P.-D. Wu, D.-H. Liu, L.-M. Zhang, and C. Xu, "Beam and image experiment of beam deflection electron gun for distributed X-ray sources," Nuclear Sci. and Techniques, vol. 30, no. 3, 2019, Art. ID 50, DOI: 10.1007/s41365-019-0561-y.

This article has been accepted for publication in a future issue of this journal, but has not been fully edited. Content may change prior to final publication. Citation information: DOI 10.1109/ACCESS.2020.3002019, IEEE Access

KONSTANTIN BULATOV (M'20) was born in Petrozavodsk, Russian Federation in 1991. He received a Specialist degree in applied mathematics from the National University of Science and Technology "MISiS", Moscow, Russia, in 2013. He obtained his Ph.D. degree in computer science in 2020 from the Federal Research Center "Computer Science and Control" of Russian Academy of Sciences, Moscow, Russia.

Since 2014 he is employed at the Federal Research Center "Computer Science and Control" of Russian Academy of Sciences, Moscow, Russia, and since 2016 he is employed at Smart Engines Service LLC, Moscow, Russia. He has been teaching a "Combinatorial optimization" course at the Moscow Institute of Physics and Technology (State University), Moscow, Russia, since 2014. He is the author of more than 20 scientific publications. His fields of study are computer vision, image processing, and document recognition systems.

MARINA CHUKALINA (M'20) was born in Cheboksary, Russia in 1965. She obtained her Masters degree in physics and mathematics in 1988 from Moscow Physical Engineering Institute, Moscow, Russia. She obtained her Ph.D. in physics in 1997 from the Institute of Microelectronics Technology and High Purity Materials of Russian Academy of Sciences, Moscow, Russia, where she has been working since 1988.

Since 2016 she is employed at the Federal Scientific Research Centre "Crystallography and Photonics" of Russian Academy of Science, Moscow, Russia, and since 2019 she is a Head of X-ray Computer Vision Department at Smart Engines Service LLC, Moscow, Russia. She is an author of over 150 papers. Her research interests include the development of signal and image processing tools for X-ray microscopy and tomography.

ALEXEY BUZMAKOV (M'20) was born in Kirs, Russia and went to the Moscow State University, where he obtained his Master degree in general physics in 2006. He received a Ph.D. degree in X-ray physics in 2009.

Since 2009 he works at the Federal Scientific Research Center "Crystallography and Photonics" of Russian Academy of Sciences, Moscow, Russia in a research group in the field of X-ray tomography and X-ray optics. Since 2019 he is also employed in the X-ray Computer Vision Department at Smart Engines Service LLC, Moscow, Russia. He is an author of more than 60 scientific publications.

DMITRY NIKOLAEV (M'20) was born in Moscow, Russia in 1978. He obtained his Masters degree in physics in 2000 from Moscow State University, Moscow, Russia and the Ph.D. degree in computer science from Moscow State University, Moscow, Russia, in 2004.

Since 2007 he has been a Head of the Vision Systems Laboratory at the Institute for Information Transmission Problems of Russian Academy of Sciences, Moscow, Russia, and since 2016 he is a CTO of Smart Engines Service LLC, Moscow, Russia. Since 2016 he also has been an Associate Professor at the Moscow Institute of Physics and Technology (State University), Moscow, Russia, teaching the "Image Processing and Analysis" course. He is an author of over 210 papers and 6 patents. His research activities are in the areas of computer vision with primary application to color image understanding.

In 2017 he lead a team of authors to win a DIBCO'17 document image binarization competition.

VLADIMIR V. ARLAZAROV (M'19) was born in Moscow, USSR in 1976. He received a Specialist degree in applied mathematics from the Moscow Institute of Steel and Alloys in 1999 and the Ph.D. degree in computer science in 2005.

Since 1999 he has been working at the Institute for Systems Analysis of Russian Academy of Sciences (currently Federal Research Center "Computer Science and Control" of Russian Academy of Sciences), Moscow, Russia, as a Researcher, Senior Researcher and Head of Laboratory. Since 2016 he is a General Director of Smart Engines Service LLC, Moscow, Russia. Since 2018 he also works at the Institute for Information Transmission Problems of Russian Academy of Sciences as a Senior Researcher, and since 2012 at the Moscow Institute of Physics and Technology (State University), Moscow, Russia, as an Associate Professor. He has published over over 70 papers and authored 5 patents. His primary fields of study are computer vision and document analysis systems.